Applied Energy 171 (2016) 256–265

Contents lists available at ScienceDirect

Applied Energy

journal homepage: www.elsevier.com/locate/apenergy

Effects of capillary-assisted tubes with different fin geometries on the performance of a low-operating pressure evaporator for adsorption cooling system applications

Poovanna Cheppudira Thimmaiah [1], Amir Sharafian [1], Wendell Huttema, Claire McCague, Majid Bahrami *

Laboratory for Alternative Energy Conversion (LAEC), School of Mechatronic Systems Engineering, Simon Fraser University, BC V3T 0A3, Canada

HIGHLIGHTS

- A low-operating pressure evaporator using capillary-assisted enhanced tubes is tested.
- Parallel fins, fin height and surface area are the main features of capillary-assisted tubes.
- Single-phase heat transfer coefficient is the bottleneck of the capillary-assisted tubes.
- Height of water column in the evaporator should be maintained below the tube diameter.
- Increasing the chilled water mass flow rate by 6.1 times increases the cooling power by 20%.

ARTICLE INFO

Article history:
Received 24 December 2015
Received in revised form 26 February 2016
Accepted 16 March 2016
Available online 22 March 2016

Keywords:
Capillary-assisted evaporation
Enhanced tube
Low-operating pressure
Adsorption cooling system
Waste heat recovery

ABSTRACT

This study investigates the performance of a low-operating pressure evaporator using capillary-assisted tubes for adsorption cooling systems (ACS). When using water as a refrigerant in an ACS, the operating pressure is low (<5 kPa) and the performance of the system is severely affected when using conventional evaporators. This problem can be addressed by using capillary-assisted evaporators. A custom-built apparatus for evaluating cooling power is used to test five types of enhanced tubes with different fin geometries. Tests were performed with 10–20 °C chilled water inlet temperatures and water vapor pressures of 0.5–0.8 kPa. The results show that the capillary-assisted tubes provide 1.6–2.2 times greater heat transfer rate compared to a plain tube. Comparing tubes with equivalent inner surface areas (0.049 m^2/m) and equivalent outer surface areas (0.193 m^2/m), and different fin heights indicates that tubes with 1.42 mm parallel continuous fins (26 fins per inch (FPI)) have a 13% higher heat transfer coefficient than those with 0.9 mm fins (40 FPI). The effects of refrigerant height, dead volume inside the evaporator and chilled water mass flow rate on the performance of evaporator are studied. The heat transfer rate increases by 65% when the water height to tube diameter ratio decreased from 1.8 to less than 1. Increasing the chilled water mass flow rate from 2.5 to 15.3 kg/min (6.1 times higher) increases evaporator heat transfer coefficient by 110%.

© 2016 Elsevier Ltd. All rights reserved.

1. Introduction

Sustainable development requires that energy utilization be balanced with environmental protection. Conventional vapor compression systems significantly increase fuel consumption and greenhouse gas production. The U.S. annually consumes about 40 billion liters of fuel for heating, ventilation, and air conditioning (HVAC) systems of light duty vehicles [1]. This makes sustainable air conditioning (A/C) systems important with regard to problems associated with conventional vapor compression refrigeration cycles (VCRCs). Thermally-driven adsorption cooling systems (ACSs) can replace VCRCs where waste heat above 60 °C is available. An internal combustion engine (ICE) of a light-duty vehicle dissipates about 40% of fuel energy in the form of high temperature exhaust gas and dissipates an additional 30% of fuel energy through the engine coolant [2]. Therefore, a VCRC of a light-duty vehicle can be replaced by an ACS, and a portion of the waste heat of the ICE could generate the cooling power required for vehicle air conditioning.

* Corresponding author at: School of Mechatronic Systems Engineering, Simon Fraser University, # 4300, 250-13450 102nd Avenue, Surrey, BC V3T 0A3, Canada.
E-mail addresses: pthimmai@sfu.ca (P. Cheppudira Thimmaiah), asharafi@sfu.ca (A. Sharafian), mbahrami@sfu.ca (M. Bahrami).

[1] Authors have contributed equally to the work.

http://dx.doi.org/10.1016/j.apenergy.2016.03.070
0306-2619/© 2016 Elsevier Ltd. All rights reserved.

Nomenclature

A	heat transfer surface area (m^2)
A/C	air conditioning
ACS	adsorption cooling system
c_p	heat capacity at constant pressure (J/kg K)
D, d	diameter (m)
ΔT_{LMTD}	log mean temperature difference (K)
FPI	fins per inch
h	heat transfer coefficient (W/(m^2 K))
ICE	internal combustion engine
k	thermal conductivity (W/(m K))
L	heat transfer length of the evaporator tube (m)
$\dot{m}$	mass flow rate (kg/s)
P	pressure (Pa)
$\dot{Q}$	total heat transfer rate (W)
$\dot{q}$	heat transfer rate (W)
r	radius (m)
T	temperature (°C)
t	time (s)
U	overall heat transfer coefficient (W/(m^2 K))
VCRC	vapor compression refrigeration cycle

Subscripts

chilled	chilled water
evap	evaporator
i	inside surface/in
o	outside surface/out
1, 2	thermocouple locations

ACS uses an adsorber bed in which an adsorbent, such as zeolite, silica gel, or activated carbon cyclically adsorbs and desorbs a refrigerant (adsorptive), such as water, methanol, or ammonia. Of these materials, water has the highest enthalpy of vaporization (latent heat), 2465.1 kJ/kg at 15 °C. However, an ACS evaporator operates between 3 and 20 °C corresponding to water saturation pressures of 0.76–2.34 kPa [3]. In this case, a conventional evaporator has poor performance.

ACS with water as the refrigerant uses a low pressure (LP) condenser and evaporator, and pressure drop can significantly affect the overall performance of the ACS. Shell-and-tube heat exchangers in which superheated water vapor flows in the shell-side of the heat exchanger and condenses on the outer surface of the tubes are commonly used for ACS LP condensers [4]. At the end of the condensation process, the liquid water accumulates at the outlet of the condenser. However, the design of a LP evaporator is different from that of a LP condenser. Accumulation of liquid water in an evaporator creates a water column, which results in a depth dependent hydrostatic pressure difference between the liquid–vapor interface and the bottom of the evaporator. For example, having a liquid water column of 5 cm in an evaporator creates a hydrostatic pressure of 0.49 kPa ($\rho_{lw} \times g \times h_{lw}$ = 1000 kg/m^3 × 9.81 m/s^2 × 0.05 m). For an evaporator operating at 1.71 kPa, this hydrostatic pressure increases the saturation temperature of water from 15 °C at the surface to 19 °C at 5 cm depth where the pressure is 2.20 kPa (1.71 + 0.49 kPa). This temperature variation in the evaporator can drastically reduce the generation of cooling power in an ACS. There are two practical approaches to minimize the negative effect of the hydrostatic pressure of water in an LP evaporator, (i) falling film evaporation, and (ii) capillary-assisted evaporation.

There are several studies investigating falling film evaporation from the outside surface of plain and enhanced (structured) tubes for refrigeration applications. Ribatski and Jacobi [5] reviewed experimental and theoretical studies of falling film evaporation and concluded that the heat transfer coefficient of enhanced tubes was up to 10 times greater than that of plain tubes. Yang and Shen [6] investigated how the heat transfer coefficient of falling films was affected by flow density, evaporation temperatures, and temperature difference between the wall and the saturated water. They showed that when the flow density was increased from 0.013 kg/(m s) to 0.062 kg/(m s), the heat transfer coefficient was increased from 5000 W/(m^2 K) to 30,000 W/(m^2 K). Li et al. [7] measured the average heat transfer coefficients of water falling films on five types of enhanced tubes, with plain tubes as a benchmark. The tests were conducted at 1 kPa and the results showed that tubes with enhanced outer and inner surfaces were required to achieve high heat transfer flux (22 kW/m^2). Li et al. [8] also tested recently commercialized enhanced tubes with 19 and 26 fins per inch (FPI) (Turbo CAB®, Wolverine Tube Inc.) and found that they provided overall heat transfer coefficients of 3000–4000 W/(m^2 K) at a falling film flow rate of 1 m^3/h and temperature of 15 °C. Their work confirmed that tubes with enhanced inner surfaces provided better heat transfer performance. While falling film evaporators can provide large cooling capacities in a low footprint, the need for equal distribution of refrigerant on horizontal tubes, parasitic power consumption (internal pump and circulator), and liquid spray equipment make falling film evaporators impractical for an ACS installed in a light-duty vehicle A/C system.

For low cooling capacities (less than 2 kW), capillary-assisted evaporators take advantage of uniform evaporation along the tubes, have no parasitic power consumption (no pump or circulator), a lower weight and less complexity. Low pressure capillary-assisted evaporation for ACS applications is relatively novel, and there are limited studies available in the literature. Capillary-assisted flow and evaporation inside a circumferential rectangular micro groove was studied by Xia et al. [9,10] for a silica gel–water ACS. A heat transfer tube with outside circumferential micro-grooves was immersed into a pool of liquid. The fluid flowing inside the tube heated the thin liquid film located in the outer micro-grooves where the liquid water rose along the micro-grooves due to capillary action and evaporated. Xia et al. also investigated the factors influencing the capillary-assisted evaporation performance, such as the immersion depth, evaporation pressure, and superheating degree. Their experimental results showed that there was a positive correlation between the evaporation heat transfer coefficient and the evaporation pressure, and negative correlation for the superheating and immersion depth. For water, i.e. at saturation temperature of 5 °C, wall superheat of 4 °C, and dimensionless liquid level (ratio of the immersion depth to tube diameter) of 0.5, the evaporation heat transfer coefficient was 3500 W/(m^2 K) and when the dimensionless liquid level was 0.25, the film side heat transfer coefficient was 5500 W/(m^2 K) [9].

Chen et al. [11] used a capillary-assisted evaporator in the experimental study of a compact silica gel–water ACS. The evaporator consisted of five trays and each tray contained nine copper tubes with outside micro-grooves. Capillary-assisted evaporation was employed in these evaporators based on Refs. [9,10]. They achieved an evaporation heat transfer coefficient of about 5000 W/(m^2 K). Lanzerath et al. [12] studied the combination of finned tubes and thermal coating for capillary-assisted evaporation at low pressures. Their investigation showed a strong dependency of the evaporation heat transfer coefficient on the filling level. Their study also established that the combination of macroscopic

fin structures and micro porous coatings yielded evaporation heat transfer coefficient of 5500 W/(m^2 K) compared with ordinary plain tubes with the evaporation heat transfer coefficient of 500 W/(m^2 K). Sabir and Bwalya [13] observed that an internally powder coated evaporator had a greater overall heat transfer coefficient compared to evaporators with deep and shallow internal grooves.

Most studies focused only on enhancing the capillary heat transfer coefficient and they do not reflect the importance of the overall heat transfer coefficient, and therefore this research attempts to fill this major void in the literature pertaining to LP evaporators. High evaporation heat transfer coefficients (4000–8000 W/(m^2 K)) can be achieved from capillary-assisted evaporation due to the water phase change on the outer surface of the tubes. The previous studies focused only on enhancing the heat transfer coefficient from the external surface of the tubes and they did not report the importance of the effects of other thermal resistances to the heat transfer. The importance of the thermal resistances has not been assessed before for LP capillary-assisted evaporation in ACS applications. To generate cooling, the heat has to be transferred from the chilled liquid water flowing inside the tube, to the tube wall, and finally, to the refrigerant. In this process, the main thermal resistance to the heat transfer is the low chilled water heat transfer coefficient (compared with the evaporation heat transfer coefficient on the outer surface of the tube) because there is no phase change. Since it is not possible to reach high heat transfer coefficient using a single-phase internal fluid, this study is focused on the overall heat transfer coefficient calculation of capillary-assisted evaporators.

In this study, five enhanced tubes with different fin geometries were tested under different operating temperatures and pressures. The main goals in this research were to find the maximum achievable cooling capacities and overall heat transfer coefficients, and to determine the most suitable tube for use in a LP evaporator. Also, a comprehensive parametric study was conducted on the selected tube under different refrigerant heights, dead volumes inside the evaporator, and chilled water flow rates. The newer enhanced tubes from Wolverine Tube Inc. (Turbo ELP, Turbo CLF, Turbo Chil-40 and 26 FPI) and Wieland Thermal Solutions (GEWA-KS-40 FPI) have not been studied before for LP capillary-assisted evaporation for ACS applications. The science behind the different regimes of cooling power as a function of liquid refrigerant height in the evaporator is one of the novel contributions of this research. LP evaporators are very critical in enhancing the performance of ACS as they do not consume parasitic energy. This research demonstrates the utilization of an LP evaporator in an ACS where low-grade waste heat energy is available.

2. Brief mechanism of capillary-assisted evaporation

Due to surface tension, the liquid–vapor interface inside the rectangular-groove creates curvature, which leads to a pressure jump across the interface. This pressure jump can be calculated by the augmented Young–Laplace equation [14]. The curvature increases gradually along the groove in the circumferential direction, creating a pressure gradient due to meniscus deformation [15], which is responsible for the upward flow of the liquid. The extended meniscus region is divided into three regions: (I) non-evaporating region, (II) evaporating thin film region, and the (III) bulk region [16]. Heat transfer is concentrated at region II where the liquid film is extremely thin and the thermal resistance is very low, creating an evaporating flow [17]. Further studies of capillary-assisted evaporation in rectangular grooves are presented in Refs. [10,15,16,18], and studies of triangular grooves can be found in Refs. [17,19].

3. Experimental details

A capillary-assisted evaporator tube with its finned outer surface in contact with a pool of liquid is schematically shown in Fig. 1. The fins draw liquid by capillary action such that the outside surface of the tube is covered. Thermal fluid (chilled water) provided by a temperature control system (TCS) is circulated inside the tube and heat is transferred to the thin liquid film on the outside of the tube leading to evaporation.

A capillary-assisted evaporator was designed and built as shown in Fig. 2. The evaporator had a four-pass arrangement with a total tube length of 1.54 m. The tube was placed horizontally at the bottom of the evaporator chamber, as shown in Fig. 2b, to minimize the required height of the water pool. The temperature, pressure, and chilled water flow rate variations in the evaporator were monitored with six Type T thermocouples with accuracy of 0.75% of reading (Omega, model #5SRTC-TT-T-36-36), a pressure transducer with 0–34.5 kPa operating range and ±0.4 kPa accuracy (Omega, model #PX309-005AI), and a positive displacement flow

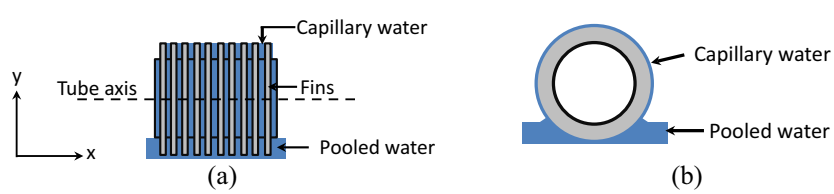

Fig. 1. Capillary-assisted evaporator tubes: (a) side view, and (b) cross-sectional view. The *x*-direction is defined to be along the axis of the tube.

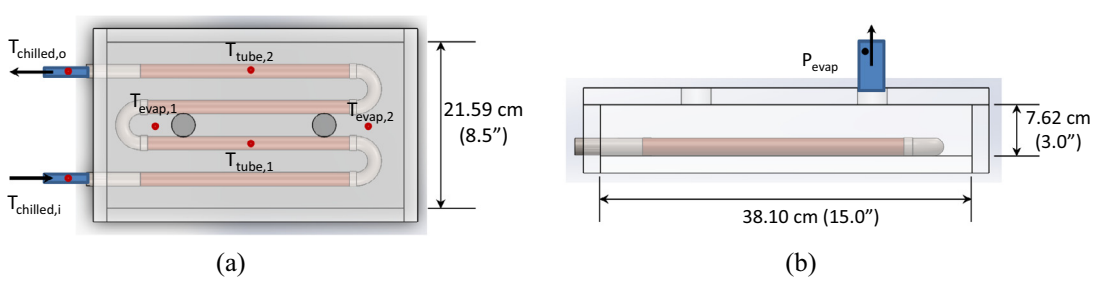

Fig. 2. Capillary-assisted evaporator built for testing different enhanced tubes: (a) top view, and (b) side view.

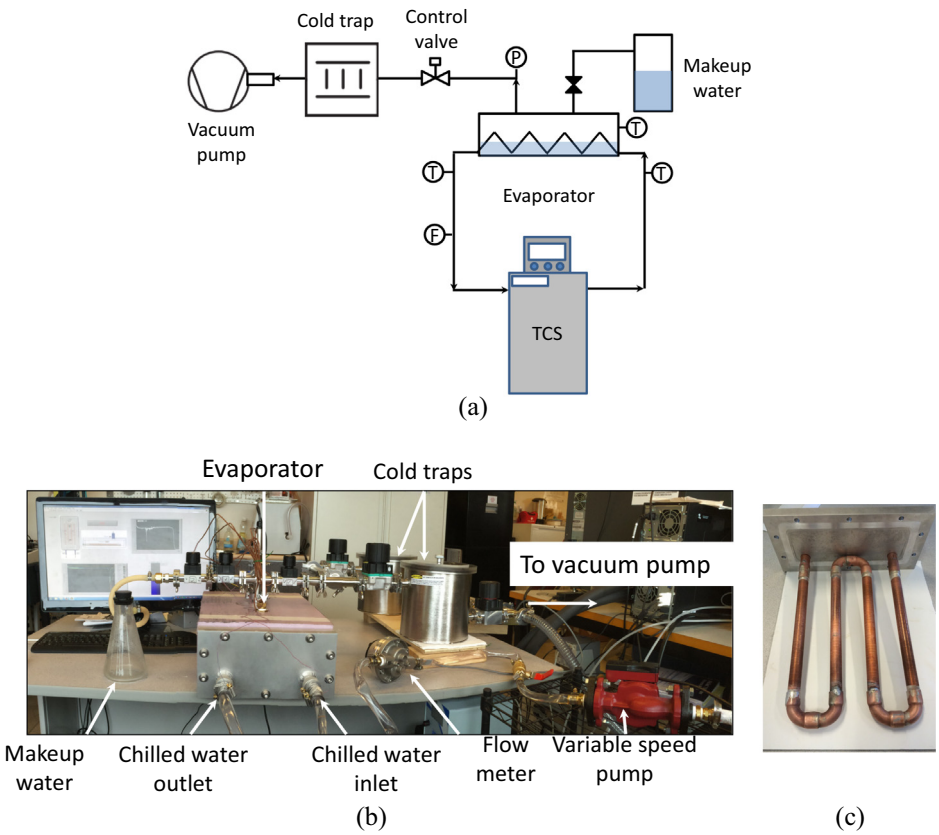

Fig. 3. (a) Schematic of the evaporator experimental setup, (b) the actual experimental setup and the main components, and (c) custom-built heat exchangers prepared for the experiments.

Table 1
Base-case operating conditions for the experiments.

Parameter	Values		
Thermal fluid (chilled water) inlet temperatures (°C)	10	15	20
Thermal fluid (chilled water) flow rate (kg/min)	2.4–2.7	2.4–2.7	2.4–2.7
Evaporator pressure (kPa)	0.5	0.6	0.8
Amount of water in the evaporator at start of experiment (g)	1200	1200	1200

meter with the accuracy of 0.5% of reading (FLOMEC, Model # OM015S001-222). The thermocouples used to measure the outside wall temperature of the tubes ($T_{tube,1}$ and $T_{tube,2}$) were in contact with top of the tube at two locations as shown in Fig. 2a. The thermocouples used to measure the liquid refrigerant temperature ($T_{evap,1}$ and $T_{evap,2}$) were placed in the refrigerant (liquid water) at positions shown in Fig. 2a, and positioned to remain submerged throughout the tests. The thermocouples were consistently placed in the same positions for tests with different tubes.

A schematic diagram and photographs of the experimental setup designed and constructed to measure the cooling capacity and overall heat transfer coefficient of evaporator tubes is shown in Fig. 3. The setup consisted of a temperature control system (TCS) and a variable speed pump to provide a constant temperature thermal fluid (chilled water) to the evaporator at different mass flow rates. Control valves were employed to regulate the pressure inside the evaporator. To protect the vacuum pump from the water vapor produced by the evaporator, two dry ice traps (cold traps) (LIT-10025, LACO Technologies) was installed before the vacuum pump. The cold traps (dry ice and IPA, −77 °C) were operated in parallel; the dry ice was replenished during the experiment; and they were able to capture the water evaporated in each experiment. The vacuum pump and cold trap in this setup were used to mimic the water vapor uptake of ACS adsorber beds with the key difference of maintaining a constant pressure (below the saturation pressure) in the evaporator.

To begin each experiment, the evaporator was evacuated, and then filled with water (1200 g) to immerse the evaporator tube in water. When the temperatures and pressure inside the evaporator became constant, the control valve was opened and adjusted until the evaporator pressure reached the specified value (0.5, 0.6 or 0.8 kPa) as per the operating conditions summarized in Table 1. Experiments began with submerged evaporator tubes, and continued through the regime where capillary evaporation maintains the evaporation heat transfer rate as the height of pooled water decreased, and ended when the evaporator chamber was dry. Tests were conducted on five types of enhanced heat transfer tubes with different fin structures and on a plain tube as a benchmark, as listed in Table 2.

4. Data analysis

The chilled water inlet and outlet temperatures, $T_{chilled,i}$ and $T_{chilled,o}$ as shown in Fig. 2a, and mass flow rate as given in Table 1, are used to calculate the heat flow rate [20] as follows:

$$\dot{q}_{evap} = \dot{m}_{chilled}\, c_{p,chilled}\, (T_{chilled,i} - T_{chilled,o}) \quad (1)$$

Table 2
Geometric details of the enhanced tubes used for the experiments.

Tube name and details	Fin structure	5× zoom view
Turbo Chil-26 FPI (Wolverine Tube Inc.) Copper Alloys C12200 Fin type: continuous and parallel fins OD: ¾″ (19.05 mm) Fin height: 1.422 mm Min. wall under fins: 0.737 mm Inside surface area: 0.049 m^2/m Outside surface area: 0.193 m^2/m	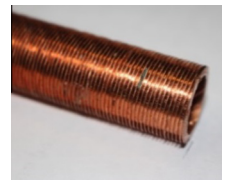	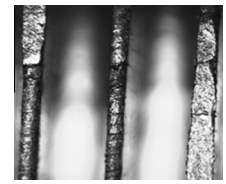
Turbo Chil-40 FPI (Wolverine Tube Inc.) Copper Alloys C12200 Fin type: continuous and parallel fins OD: ¾″ (19.05 mm) Fin height: 1.473 mm Min. wall under fins: 0.635 mm Inside surface area: 0.051 m^2/m Outside surface area: 0.263 m^2/m		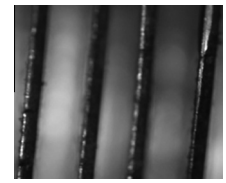
Turbo ELP (Wolverine Tube Inc.) Copper Alloys C12200 Fin type: interrupted micro pin fins OD: ¾″ (19.05 mm) Fin height: 0.5 mm Min. wall under fins: 0.889 Inside surface area: 0.073 m^2/m Outside surface area: 194.8 m^2/m		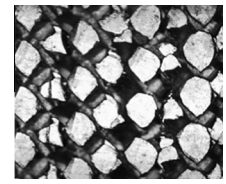
Turbo CLF-40 FPI (Wolverine Tube Inc.) Copper Alloys C12200 Fin type: continuous with interrupted cross heads on top of the fin OD: ¾″ (19.05 mm) Fin height: 0.965 mm Min. wall under fins: 0.787 mm Inside surface area: 0.0549 m^2/m Outside surface area: 0.2173 m^2/m		
GEWA-KS-40 FPI (Wieland Thermal Solutions) Copper Alloys C12200 Fin type: continuous and parallel fins OD: ¾″ (19.05 mm) Fin height: 0.9 mm Min. wall under fins: 0.7 mm Inside surface area: 0.0489 m^2/m Outside surface area: 0.194 m^2/m		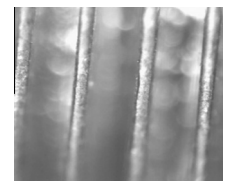
Plain Tube Copper Alloys C12200 OD: ¾″ (19.05 mm) Inside surface area: 0.0547 m^2/m Outside surface area: 0.0598 m^2/m		

The total evaporation rate is calculated by time averaging the heat flow rate given in Eq. (1):

$$\dot{Q}_{evap} = \frac{\int_{t_1}^{t_2} \dot{q}_{evap}\, dt}{t_2 - t_1} \tag{2}$$

where t_1 and t_2 are the beginning and end of the time when the temperatures in the evaporator are constant. Finally, the overall evaporator heat transfer conductance, *UA* is

$$UA = \frac{\dot{Q}_{evap}}{\Delta T_{LMTD}} \tag{3}$$

where the logarithmic mean temperature difference between the chilled water circuit and the refrigerant is calculated by

$$\Delta T_{LMTD} = \frac{T_{chilled,i} - T_{chilled,o}}{\ln\left(\frac{T_{chilled,i} - T_{evap}}{T_{chilled,o} - T_{evap}}\right)} \tag{4}$$

where T_{evap} is the average of the evaporation temperatures $T_{evap,1}$ and $T_{evap,2}$ as shown in Fig. 2a. A_{evap} is chosen as the outside heat transfer surface area of the plain tube in order to having a reference (nominal) surface area for the calculation of U_{evap} for all tubes.

The systematic uncertainty [21] in the evaporator heat transfer rate calculation, Eq. (1), is:

$$\left(\frac{\delta \dot{q}_{evap}}{\dot{q}_{evap}}\right)_{systematic} = \sqrt{\left(\frac{\delta \dot{m}_{chilled}}{\dot{m}_{chilled}}\right)^2 + \left(\frac{\delta(T_{chilled,i} - T_{chilled,o})}{T_{chilled,i} - T_{chilled,o}}\right)^2} \tag{5}$$

where

$$\frac{\delta(T_{chilled,i} - T_{chilled,o})}{T_{chilled,i} - T_{chilled,o}} = \sqrt{\left(\frac{\delta T_{chilled,i}}{T_{chilled,i}}\right)^2 + \left(\frac{\delta T_{chilled,o}}{T_{chilled,o}}\right)^2} = \sqrt{0.0075^2 + 0.0075^2} = 0.01 \tag{6}$$

Thus, the maximum systematic uncertainty in the calculation of evaporator heat transfer rate is:

$$\left(\frac{\delta \dot{q}_{evap}}{\dot{q}_{evap}}\right)_{systematic} \times 100 = \sqrt{0.005^2 + 0.01^2} = 1.1\% \tag{7}$$

Also, the standard deviation for $\dot{q}_{evap}$ due to the random uncertainty is 4.2%. Thus the maximum uncertainty of $\dot{q}_{evap}$ during the experiments is 5.3% (=1.1% + 4.2%). The systematic uncertainty of the evaporation heat transfer rate is

$$\left(\frac{\delta U_{evap}}{U_{evap}}\right)_{systematic} = \sqrt{\left(\frac{\delta \dot{Q}_{evap}}{\dot{Q}_{evap}}\right)^2_{systematic} + \left(\frac{\delta \Delta T_{LM,evap}}{\Delta T_{LM,evap}}\right)^2} \quad (8)$$

where $\left(\frac{\delta \dot{Q}_{evap}}{\dot{Q}_{evap}}\right)_{systematic}$ and $\frac{\delta \Delta T_{LM,evap}}{\Delta T_{LM,evap}}$ are equal to 1.1% and 0.04%, respectively. Therefore, $\left(\frac{\delta U_{evap}}{U_{evap}}\right)_{systematic}$ is equal to 1.1% (≈(1.1% + 0.04%). The random uncertainty in the measurement for U_{evap} over time is 7.4%. Thus, the maximum uncertainty in the calculation of evaporator heat transfer coefficient is 8.5% (=1.1% + 7.4%).

5. Results and discussion

5.1. Base-case operating condition

Fig. 4 shows the operating pressure and temperatures of the evaporator with a fin height of 1.473 mm and 40 FPI (Turbo Chil-40 FPI) for a constant 15 °C thermal fluid inlet temperature. As shown in Fig. 4a, when the control valve between the evaporator and the cold trap is opened, the evaporator pressure decreases, and then remains constant until the evaporator runs out of water. The six thermocouples read 15 °C at the start of the experiment. After the valve is opened, the temperature of the tubes and refrigerant drop as shown in Fig. 4b. The total heat transfer rate and the evaporator heat transfer coefficient are calculated from the steady state data from the region demarcated in gray in Fig. 4. In Fig. 5, the performance of this evaporator is compared with one built from plain tubes. The Turbo Chil-40 FPI tube has a heat transfer coefficient of 767 W/(m^2 K) compared to 308 W/(m^2 K) for the plain tube. As shown in Fig. 5a and b, the capillary phenomenon on the finned tubes results in an almost constant evaporation heat transfer rate and, consequently, constant evaporator heat transfer coefficient over time. As the height of the liquid water decreases, the capillary action continues to cover the entire outside surface of the tube. Fig. 5c and d shows that the heat transfer rate and the heat transfer coefficient for the plain tube drop as a function of time. With the plain tube, as the height of the liquid water inside the evaporator decreases, the area of the tube surface in contact with the water decreases, and this results in a decrease in the heat transfer rate and heat transfer coefficient.

To evaluate the performance of tubes with the five distinct fin types listed in Table 2, each tube type was tested with thermal fluid inlet temperatures of 10, 15, and 20 °C under the operating conditions summarized in Table 1. The total heat transfer rates and the heat transfer coefficients of the evaporator with each fin type are shown in Fig. 6. The enhanced tubes had heat transfer rates significantly greater than that of the plain tube. The evaporator with fin height of 1.473 mm and 40 FPI (Turbo Chil-40 FPI) provided the highest total heat transfer rate, 422 W, when operated at 20 °C, followed by Turbo Chil-26 FPI and Turbo ELP-42 FPI. The evaporator with Turbo Chil-40 FPI tubes had an overall heat transfer coefficient ranging from 596 to 888 W/(m^2 K) when operated with inlet temperatures of 10–20 °C, as shown in Fig. 6b. While for the plain tube evaporator the heat transfer coefficient varies from 285 to 365 W/(m^2 K).

Comparing the evaporator heat transfer coefficients of the enhanced tubes, as shown in Fig. 6b, indicates that having continuous parallel fins, such as Turbo Chil-40 FPI and Turbo Chil-26 FPI, and high heat transfer surface area, such as Turbo ELP, are the two most important parameters in the design of capillary-assisted evaporators. The evaporator with 1.422 mm fin height and 26 FPI tubes (Turbo Chil-26 FPI) had a greater heat transfer coefficient than the one with 0.9 mm fin height and 40 FPI (GEWA-KS-40 FPI) despite having identical internal and external heat transfer surface areas, indicating the importance of fin height to capillary action. Thus, the main features of an enhanced tube designed for capillary-assisted evaporator are: (i) continuous parallel fins, (ii) high fin height, and (iii) high heat transfer surface area. As a result, it can be concluded that the evaporator built with Turbo Chil-40 FPI for ACS provides the highest cooling power compared with the other enhanced tubes.

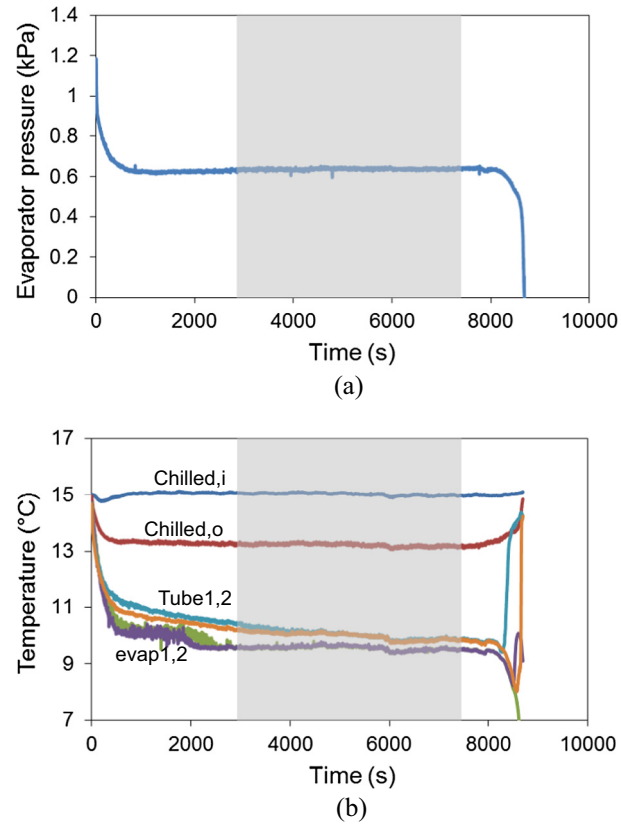

Fig. 4. The behavior of evaporator with 1.47 mm, 40 FPI tubes (Turbo Chil-40 FPI) at the thermal fluid (chilled water) inlet temperature of 15 °C vs. time: (a) evaporator pressure operated from flooded to dry and (b) temperature at different locations in the evaporator.

The internal heat transfer coefficient can be calculated by following expression [22]:

$$\frac{1}{UA} = \left(\frac{1}{h_o A_o} + \frac{1}{h_i A_i} + R_{o,finned\,tube}\right) \quad (9)$$

The first term on the right hand side of Eq. (9) describes the external convective heat resistance due to capillary evaporation, the second term is the internal convective heat resistance due to single phase flow inside the tube, and the third term is the conductive heat resistance of the tube wall. From the analysis shown in Appendix A, the internal convective heat resistance can be calculated. As summarized in Table 3, 91.3% of the overall thermal resistance of Turbo Chil-40 FPI tubes is due to the internal convective resistance, while the conductive resistance of tube and external convective resistance contribute only 4.7% and 4.0% of the overall thermal resistance, respectively.

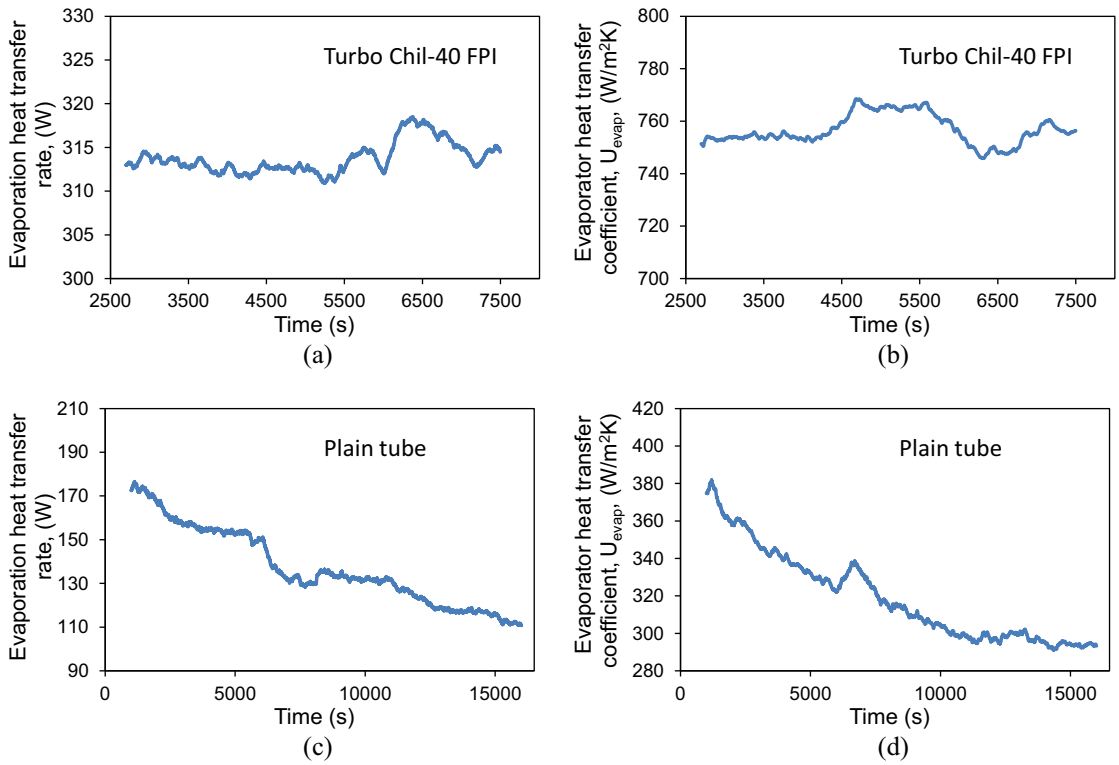

Fig. 5. Effect of capillary phenomenon on the performance of the LP evaporator vs. time. Heat transfer rate and evaporator heat transfer coefficient achieved by using (a) and (b) 1.47 mm, 40 FPI tubes (Turbo Chil-40 FPI), and (c) and (d) plain tubes. For the evaporator heat transfer coefficient, the plain tube surface area is $A = 9.22 \times 10^{-2}$ m^2.

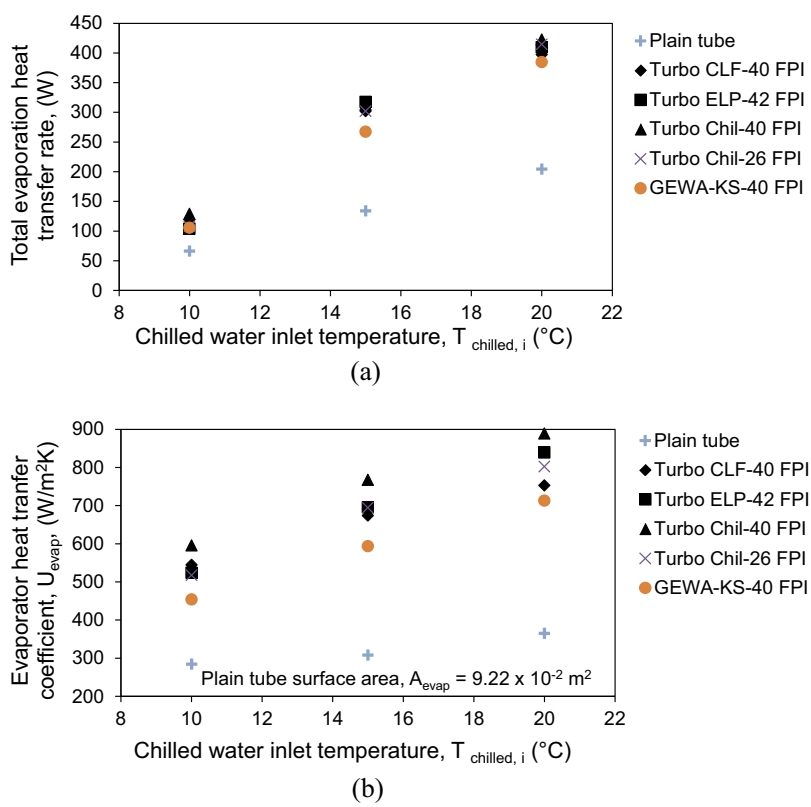

Fig. 6. The total heat transfer rate (a) and the evaporator heat transfer coefficient (b) of evaporators with five different outer surface fin structure compared to plain tubes as function of thermal fluid (chilled water) temperature.

5.2. Parametric study

In this section, the effects of water height, dead volume inside the evaporator, and thermal fluid (chilled water) mass flow rate on the performance of the evaporator built with Turbo Chil-40 FPI are studied. To test the effect of water height on the performance, the evaporator was filled with 2.4 kg of water to submerge the tubes by ~2 cm as shown in Fig. 7b. Fig. 7a shows the varia-

Table 3
Conductive and Convective resistances at different thermal conductivities.

Tube material	Wall thermal conductivity (W/m K)	Ext. convection resistance (K/W)	Conductive resistance (K/W)	Int. convection resistance (K/W)	Overall thermal resistance (K/W)
Copper Alloys C12200	340	4.87×10^{-4}	5.78×10^{-4}	1.12×10^{-2}	1.23×10^{-2}

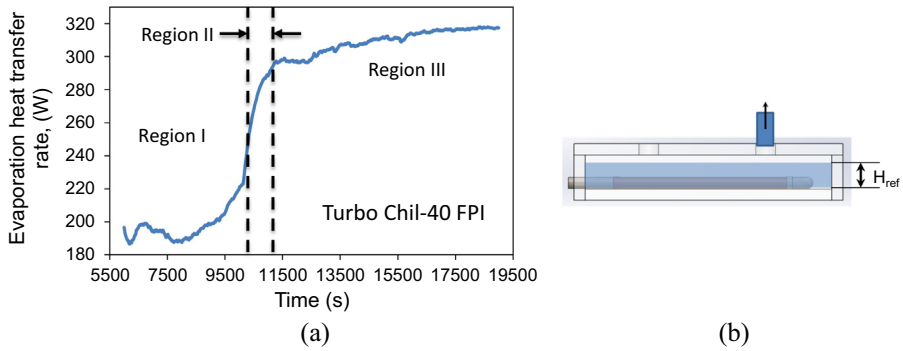

Fig. 7. (a) Effect of water height variation on the performance of capillary-assisted evaporator with 1.47 mm, 40 FPI tubes (Turbo Chil-40 FPI) over time at chilled water inlet temperature of 15 °C and mass flow rate of 2.53 kg/min, (b) schematic of the evaporator filled with 2.4 kg of water to submerge the tubes by ~2 cm. H_{ref} = 34.7 mm, D_{tube} = 19.05 mm.

tions of heat transfer rate as a function of water height versus time during operation with $T_{chilled,i}$ of 15 °C and a mass flow rate of 2.53 kg/min. The evaporation heat transfer rate is divided into three regions: region I (tube is fully submerged), region II (transition region), and region III (water height is lower than the tube diameter and the capillary evaporation is in effect). In region I, evaporation heat transfer rate is about 200 W. In this region, the hydrostatic pressure creates a pressure gradient between liquid water–vapor interface and the bottom of the evaporator. As a result, saturation temperature of water increases at the bottom of the evaporator, decreases the temperature difference between the chilled water circulated inside the tube and the water (refrigerant) located outside the tube, reducing the cooling power. When evaporation lowers the water level to the height of the tube diameter, the hydrostatic pressure is reduced and the heat transfer rate increases from 220 to 300 W (region II). In region III, the heat transfer rate remains high as the water level decreases further due to thin film capillary evaporation. The heat transfer coefficient of the evaporation was 568 W/(m^2 K) in region I, and increased to 767 W/(m^2 K) in region III.

The effect of water non-dimensional height, H^*, inside the evaporator on the total evaporation heat transfer rate and evaporator heat transfer coefficient is shown in Fig. 8. H^* represents the ratio of water (refrigerant) height to the tube diameter. Fig. 8a shows that by increasing H^* from one to 1.8 (80% increase), the total evaporation heat transfer rate reduces by 25% from 313 W to 250 W. Accordingly, the evaporator heat transfer coefficient reduced by 33% as shown in Fig. 8b.

In order to determine whether the dead volume inside the evaporator affects the performance, an acrylic block was placed above the tubes to reduce the interior volume of the evaporator by 25% as schematically shown in Fig. 9. The evaporator was tested with and without the filler block, operating with thermal fluid $T_{chilled,i}$ of 15 °C and $\dot{m}_{chilled,i}$ of 2.53 kg/min, and starting with 1.2 kg of water. Calculating from steady state operating temperatures (i.e. after the initial period in which the thermal inertia of the evaporator impacts refrigerant temperature), it was found that reducing the interior volume of the evaporator decreased the heat transfer rate by 2.3% and the heat transfer coefficient by 10%. The slight change observed in the heat transfer rate was within the uncertainty of the test and may reflect a small increase, due to the filler block, in the mass transfer resistance for water vapor leaving the evaporator.

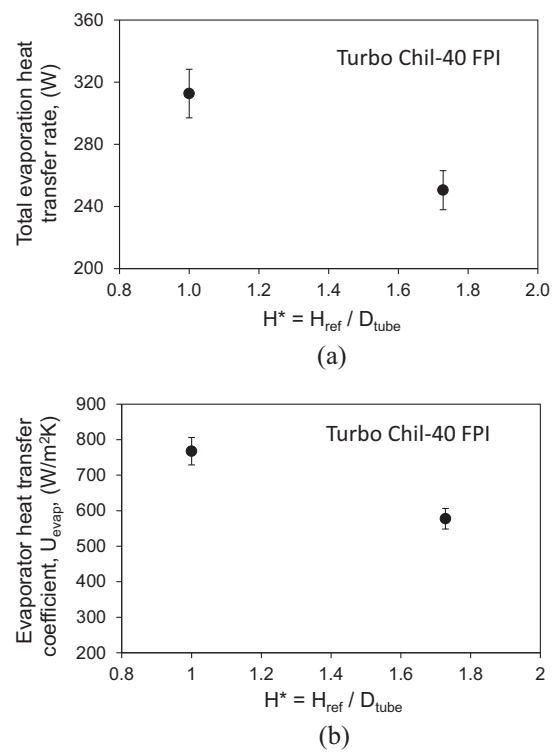

Fig. 8. Effect of water non-dimensional height, H^*, on (a) total evaporation heat transfer rate and (b) evaporator heat transfer coefficient of capillary-assisted evaporator with 1.47 mm, 40 FPI tubes (Turbo Chil-40 FPI), D_{tube} = 19.05 mm at thermal fluid (chilled water) inlet temperature of 15 °C and mass flow rate of 2.53 kg/min. For the evaporator heat transfer coefficient, the plain tube surface area is $A = 9.22 \times 10^{-2}$ m^2.

Xia et al. measured heat transfer coefficients ranging from 4000 to 8000 W/(m^2 K) for capillary evaporation of water on finned tubes around the circumference of the tubes [9,10]. However, the single-phase heat transfer from the thermal fluid inside the tube to the refrigerant on the surface of the tube, where heat transfer

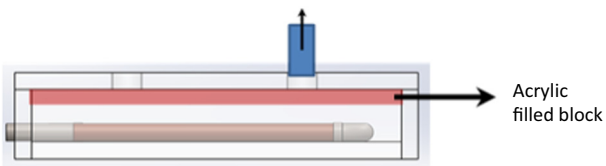

Fig. 9. Schematic showing how dead volume inside the evaporator was changed using an acrylic block.

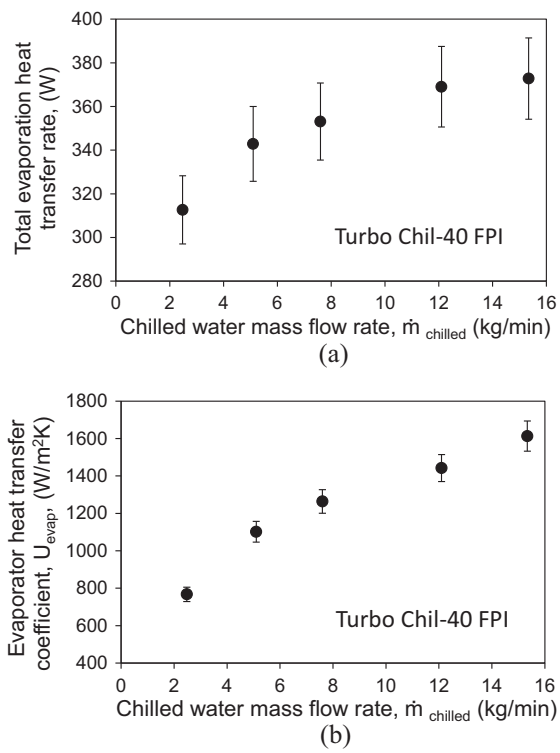

Fig. 10. Effect of chilled water mass flow rate on (a) total evaporation heat transfer rate and (b) evaporator heat transfer coefficient for a capillary-assisted evaporator with 1.47 mm, 40 FPI tubes (Turbo Chil-40 FPI) at thermal fluid (chilled water) inlet temperature of 15 °C. For the evaporator heat transfer coefficient, the plain tube surface area is $A = 9.22 \times 10^{-2}$ m^2.

with phase-change occurs, is always limited by the heat transfer conductance of the thermal fluid (chilled water, h_iA_i). The evaporator heat transfer coefficient can be increased by increasing the flow rate inside the tube. The effect of thermal fluid mass flow rate on the total heat transfer rate and evaporator heat transfer coefficient was measured using the evaporator with Turbo Chil-40 FPI tube. It can be seen in Fig. 10 that increasing the mass flow rate from 2.5 kg/min to 15.3 kg/min (6.1 times) increases the total evaporation heat transfer rate by from 313 W to 373 W (20%), and the evaporator heat transfer coefficient increases from 767 W/(m^2 K) to 1613 W/(m^2 K) (110%). However, higher thermal fluid mass flow rates require higher water pump power consumption, which is a consideration for overall ACS system designs.

6. Conclusions

Five types of capillary-assisted tubes were evaluated for a low pressure evaporator for ACS. The evaporator consisted of horizontal capillary-assisted tubes that were in contact with a pool of water while the pressure in the evaporator was maintained at 0.5, 0.6 or 0.8 kPa for tests with thermal fluid inlet temperatures of 10, 15 and 20 °C, respectively. The total heat transfer rate and heat transfer coefficient of evaporators with a plain tube and five different enhanced tubes with various surface geometries were experimentally investigated. The experimental results indicated that Turbo Chil-40 FPI provided the highest heat transfer rate and evaporator heat transfer coefficient. The main findings of this study are summarized below:

- Tubes with continuous parallel fins on their outer surfaces had significantly higher heat transfer rate and heat transfer coefficients relative to plain tubes.
- Experimental analyses indicated that the evaporator performance was limited by the heat transfer resistance of the thermal fluid (chilled water) flowing inside the tubes.
- Increasing the thermal fluid (chilled water) mass flow rate from 2.5 kg/min to 15.3 kg/min (6.1 times) increased the total evaporation heat transfer rate and evaporator heat transfer coefficient by 20% and 110%, respectively.
- To achieve the highest heat transfer rate, the refrigerant (water) height in the evaporator had to be less than the tube diameter.
- The interior volume above the enhanced tubes of the capillary-assisted evaporator did not have a significant effect on evaporator performance.

Following the detailed evaluation of low pressure evaporators, the evaporator with the highest performing capillary-assisted tubes (Turbo Chil-40 FPI) was used in tests of a lab-scale ACS system [23]. A low pressure evaporator with smaller tube diameters and a header designed to decrease tube spacing and maximize overall heat transfer length has also been constructed and tested.

Acknowledgments

The authors gratefully acknowledge the financial support of the Natural Sciences and Engineering Research Council of Canada (NSERC) through the Automotive Partnership Canada Grant No. APCPJ 401826-10. Authors are thankful to Wolverine Tube Inc. and Wieland Thermal Solutions for assisting our research by providing tube samples. Authors are also thankful to Mr. Ameer Ismail for his kind support in conducting the experiments in the laboratory.

Appendix A

To calculate the internal convective resistance due to a fluid circulated in a finned tube, the following steps should be taken. The tube of interest in this analysis is a Turbo Chil-40 FPI with circumferential, rectangular cross-section fins. The efficiency of a fin located on the surface of the tube can be calculated from Eqs. (A1)–(A5) [22]

$$\eta_f = C\left(\frac{K_1(mr_1)I_1(mr_{2c}) - I_1(mr_1)K_1(mr_{2c})}{I_0(mr_1)K_1(mr_{2c}) + K_0(mr_1)I_1(mr_{2c})}\right) \quad \text{(A1)}$$

$$C = \frac{(2r_1/m)}{(r_{2c}^2 - r_1^2)} \quad \text{(A2)}$$

$$m = \sqrt{\left(\frac{2h}{kt_f}\right)} \quad \text{(A3)}$$

$$r_{2c} = r_2 + (t_f/2) \quad \text{(A4)}$$

$$A_f = 2\pi(r_{2c}^2 - r_1^2) \quad \text{(A5)}$$

where r_1 and r_2 are the distances from the center of the tube to the fin base and fin tip, respectively. I_0, and K_0 in Eq. (A1) are modified, zero-order Bessel functions of the first and second kinds, respectively. I_1, and K_1 in Eq. (A1) are modified, first-order Bessel functions of the first and second kinds, respectively. t_f in Eq. (A3) is the fin

Table A1
Detailed geometry of Turbo Chil-40 FPI tubes.

Parameter	Value
L	1.54 m
r_0	7.417×10^{-3} m
r_1	8.052×10^{-3} m
r_2	9.525×10^{-3} m
t_f	1.59×10^{-4} m
t_b	4.76×10^{-4} m
h_o	5000 W/m^2 K
k	340 W/m K
A_t	0.41 m^2
A	0.0922 m^2
A_i	0.0796 m^2

thickness and A_f in Eq. (A5) is the fin heat transfer surface area. The total external heat transfer surface area of the finned tube is calculated as follows:

$$A_t = N(A_f + A_b) \tag{A6}$$

$$A_b = 2\pi r_1 t_b \tag{A7}$$

where N is the total number of fins, and A_b and t_b are the prime (plain) heat transfer surface area of the finned tube and the space between two fins, respectively. Using Eqs. (A1), (A5), and (A6) the overall efficiency of the finned tube can be calculated [22]:

$$\eta_{o,fin} = 1 - \frac{A_f}{A_f + A_b}(1 - \eta_f) \tag{A8}$$

Consequently, the conductive heat transfer resistance due to the fins of the finned tube can be estimated.

$$R_{fin} = \frac{1}{\eta_{o,fin} h_o A_t} \tag{A9}$$

where the convection coefficient of h_o is measured from experimentations. Also, the conductive resistance of wall located under the fins can be calculated as follows:

$$R_{wall} = \frac{\ln(r_1/r_0)}{2\pi k L} \tag{A10}$$

where r_0 and L are the internal radius and length of the finned tube, respectively. R_{fin} and R_{wall} are thermal resistances in series. Therefore, the overall conductive resistance of the finned tube is calculated by Eq. (A11).

$$R_{o,finned\,tube} = R_{fin} + R_{wall} \tag{A11}$$

Finally, Eq. (A12) gives the internal convective heat transfer resistance of the finned tube.

$$\frac{1}{h_i A_i} = \frac{1}{UA} - \left(\frac{1}{h_o A_o} + R_{o,finned\,tube}\right) \tag{A12}$$

From the experimental data of Xu et al. [9], the capillary evaporation coefficient on the external surface of a finned tube varies between 4000 and 6000 W/(m^2 K). Information required to calculate the internal convective resistance of a Turbo Chil-40 FPI tube is listed in Table A1.

By substituting the values given in Table A1, a fin efficiency, η_f, is 0.86 and the overall efficiency of the finned tube, $\eta_{o,fin}$, is 0.88. Using these data, the conductive resistance of the tube and internal convective resistance of the finned tube can be calculates as shown in Table 3.

References

[1] Farrington R, Rugh J. Impact of vehicle air-conditioning on fuel economy, tailpipe emissions, and electric vehicle range. Fuel 2000. <http://www.nrel.gov/docs/fy00osti/28960.pdf>.
[2] Suzuki M. Application of adsorption cooling systems to automobiles. Heat Recover Syst CHP 1993;13:335–40.
[3] Schnabel L, Witte K, Kowol J, Schossig P. Evaluation of different evaporator concepts for thermally driven sorption heat pumps and chiller. In: Int sorption heat pump conf, Padua, Italy; 2011. p. 525–43.
[4] Wang RZ, Wang L, Wu J. Adsorption refrigeration technology: theory and application. John Wiley & Sons; 2014.
[5] Ribatski G, Jacobi AM. Falling-film evaporation on horizontal tubes – a critical review. Int J Refrig 2005;28:635–53. http://dx.doi.org/10.1016/j.ijrefrig.2004.12.002.
[6] Yang L, Shen S. Experimental study of falling film evaporation heat transfer outside horizontal tubes. Desalination 2008;220:654–60. http://dx.doi.org/10.1016/j.desal.2007.02.046.
[7] Li W, Wu XY, Luo Z, Yao SC, Xu JL. Heat transfer characteristics of falling film evaporation on horizontal tube arrays. Int J Heat Mass Transfer 2011;54:1986–93. http://dx.doi.org/10.1016/j.ijheatmasstransfer.2010.12.031.
[8] Li W, Wu XY, Luo Z, Webb RL. Falling water film evaporation on newly-designed enhanced tube bundles. Int J Heat Mass Transfer 2011;54:2990–7. http://dx.doi.org/10.1016/j.ijheatmasstransfer.2011.02.052.
[9] Xia ZZ, Yang GZ, Wang RZ. Experimental investigation of capillary-assisted evaporation on the outside surface of horizontal tubes. Int J Heat Mass Transfer 2008;51:4047–54. http://dx.doi.org/10.1016/j.ijheatmasstransfer.2007.11.042.
[10] Xia ZZ, Yang GZ, Wang RZ. Capillary-assisted flow and evaporation inside circumferential rectangular micro groove. Int J Heat Mass Transfer 2009;52:952–61. http://dx.doi.org/10.1016/j.ijheatmasstransfer.2008.05.041.
[11] Chen CJ, Wang RZ, Xia ZZ, Kiplagat JK, Lu ZS. Study on a compact silica gel–water adsorption chiller without vacuum valves: design and experimental study. Appl Energy 2010;87:2673–81. http://dx.doi.org/10.1016/j.apenergy.2010.03.022.
[12] Lanzerath F, Erdogan M, Schreiber H, Steinhilber M, Bardow A. Combination of finned tubes and thermal coating for high performance water evaporation in adsorption heat pumps. In: Int sorption heat pump, College Park, MD, USA; 2014. p. 1–10.
[13] Sabir HM, Bwalya AC. Experimental study of capillary-assisted water evaporators for vapour-absorption systems. Appl Energy 2002;71:45–57. http://dx.doi.org/10.1016/S0306-2619(01)00042-3.
[14] Panchamgam SS, Plawsky JL, Wayner PC. Microscale heat transfer in an evaporating moving extended meniscus. Exp Therm Fluid Sci 2006;30:745–54. http://dx.doi.org/10.1016/j.expthermflusci.2006.03.004.
[15] Nilson RH, Tchikanda SW, Griffiths SK, Martinez MJ. Steady evaporating flow in rectangular microchannels. Int J Heat Mass Transfer 2006;49:1603–18. http://dx.doi.org/10.1016/j.ijheatmasstransfer.2005.11.002.
[16] Ma HB, Cheng P, Borgmeyer B, Wang YX. Fluid flow and heat transfer in the evaporating thin film region. Microfluid Nanofluid 2008;4:237–43. http://dx.doi.org/10.1007/s10404-007-0172-5.
[17] Ma HB, Peterson GP. Temperature variation and heat transfer in triangular grooves with an evaporating film. J Thermophys Heat Transfer 1997;11:90–7. http://dx.doi.org/10.2514/2.6205.
[18] Cheng P, Dong J, Thompson SM, Ma HB. Heat transfer in the bulk and thin film fluid regions of a rectangular micro groove. J Thermophys Heat Transfer 2012;26:108–14. http://dx.doi.org/10.2514/1.T3684.
[19] Chiang D-Y, Huang S-T, Xu X, Carey VP. Film evaporation from a micro-grooved surface – an approximate heat transfer model and its comparison with experimental data. J Thermophys Heat Transfer 1990;4:512–20. http://dx.doi.org/10.2514/3.215.
[20] Holman JP. Heat transfer. 10th ed. McGraw-Hill Education; 2010.
[21] Holman JP. Experimental methods for engineers. 8th ed. McGraw-Hill Education; 2012.
[22] Bergman TL, Lavine AS, Incropera FP, DeWitt DP. Introduction to heat transfer. 6th ed. John Wiley & Sons; 2011.
[23] Sharafian A, Nemati Mehr S, Cheppudira Thimmaiah P, Huttema W, Bahrami M. Effects of adsorbent mass and number of adsorber beds on the performance of a waste-heat driven adsorption cooling system for vehicle air conditioning applications. Energy 2016 [revised].